Reaction Kinetics, Mechanisms and Catalysis (2023) 136:2815–2834
https://doi.org/10.1007/s11144-023-02472-2

Impact of quercetin concentration on the thermal stability of ultra high molecular weight polyethylene: a thermogravimetric study

Nidhi Khattar[1] · Jagriti[1] · Piyush Sharma[2] · Vishal Ahlawat[3] · Urmila Berar[1] · P. K. Diwan[1]

Received: 6 June 2023 / Accepted: 11 August 2023 / Published online: 21 August 2023

Abstract

The impact of quercetin concentration (0.1–1.0 wt%) on the thermal stability of Ultra high molecular weight polyethylene (UHMWPE), in temperature region 50–600 °C, at 5 °C/min is examined by utilizing the thermogravimetric (TGA/DTA) technique. The activation energies of these thermograms are determined by utilizing the model fitting kinetic method (Coats and Redfern). Through this, 0.4 wt% is found to be the optimum quercetin concentration. UHMWPE sample at optimized quercetin concentration is further subjected to three other heating rates (10, 15 and 20 °C), in same temperature region. The complexities involved in thermal decomposition are resolved by using the deconvolution technique, adopting a bi-Gaussian asymmetric function. Activation energies of these deconvoluted peaks, obtained through Starink and Friedman kinetic models, follow a similar trend. By utilizing activation energy, a random nucleation reaction mechanism involved in thermal decomposition is identified. Finally, the pre-exponential factor, change in entropy (ΔS), change in enthalpy (ΔH) and change in Gibbs free energy (ΔG) are determined.

Keywords UHMWPE · Quercetin · Reaction mechanism · Kinetic triplets · Deconvolution · Thermodynamic parameters

✉ P. K. Diwan
diwanpk74@gmail.com

[1] Department of Applied Science, UIET, Kurukshetra University, Kurukshetra 136119, India

[2] Thapar Institute of Engineering and Technology, Virginia Tech Center of Excellence in Emerging Materials, Patiala 147004, India

[3] Department of Mechanical Engineering, UIET, Kurukshetra University, Kurukshetra 136119, India

Introduction

In engineering applications where friction and wear are a major concern, ultra high molecular weight polyethylene (UHMWPE) is a highly preferred polymer due to its excellent wear resistance, biocompatibility, low friction and chemical inertness [1–6]. As a linear semi-crystalline polymer, it has both crystalline and amorphous phases. Chains are folded into highly oriented lamellae of thickness 10–50 nm and length 10–50 µm in the crystalline phase. In the amorphous phase, the lamellae are arranged randomly and are connected to each other through tie molecules [7]. UHMWPE is widely utilized in a wide range of applications like automotive, engineering bearings and as bio-implant materials in artificial joints etc. [8–12].

Despite of its unique characteristics, UHMWPE cannot be used in high temperature applications due to its low thermal stability. As per previous researches [13, 14], thermal stability can be improved by increasing the tendency of cross-linking of molecular chains in the polymer. Generally, this is achieved by irradiating UHMWPE with gamma or electron-beam (EB) radiations [15–18]. Gamma radiation dependent cross-linking is highly significant to design synthetic joints because it can also sterilize the material and thereby removing bacterial contamination [19]. C–C and C–H bonds in UHMWPE are breakdown by means of energetic gamma/EB radiations and formed alkyl radicals [20]. These radicals react with each other and also with unsaturated bonds in the polymer and as a result, cross-linking occurs. Due to irradiation, radicals are formed in both the amorphous and crystalline phase in the material. In the amorphous phase, free radicals tend to quench within 10 h or induce cross linking, while in the crystalline phase, free radicals can remain active up to eight years and migrate into amorphous phase causing embrittlement and as a result shows unexpected failure in UHMWPE [21, 22].

In order to overcome this problem, post-irradiation thermal treatment (re-melting or annealing) is utilized to remove free radicals trapped in the crystalline phase and precursor to oxidative degradation [23, 24]. However, such thermal treatment decreases the crystallinity and ductility of UHMWPE and thus sacrifices with the strength, toughness and fatigue, which results in cracking within a short period of time after its usage [22]. Another alternative treatment is the addition of antioxidants in a polymer matrix, which results in a promising alternative strategy for scavenging free radicals trapped in the crystalline phase [25].

Antioxidants, mainly hindered phenol, do not completely eliminate oxidative degradation, but they substantially inhibit the rate of auto oxidation by interfering with the radical propagation reaction [26]. Conventionally, a synthetic antioxidant such as 2,6-di-tertiary-butyl-4-methyl phenol (BHT), tertiary-butyl-4-hydroxy-anisole (BHA), tertiary-butyl-hydroquinone (TBHQ), and 6-ethoxy-1,2-dihydro-2,4-trimethylquinoline (ethoxyquin, EQ) are used to enhance the thermal stability of UHMWPE[27–31]. However, these synthetic antioxidants are toxic in nature and have harmful effects on the human body. Therefore, natural antioxidants (Gallic acid, Dodecy gallate, Vitamin C and Vitamin E) are recommended due to

their non-toxic and negligible harmful effects [32, 33]. Vitamin E (α-tocopherol) is proven to be a successful natural antioxidant applied to stabilize UHMWPE by donating a proton of phenolic HO˚ to a macro-radical and itself becoming a much less reactive phenoxy radical due to the delocalization of unpaired electron over the aromatic ring. Intensive research resulted in the application of α-tocopherol for stabilizing UHMWPE, which was used as a joint implant. Even an ASTM standard specification suggested UHMWPE blended with Vitamin E for medical and other applications [33].

Quercetin, a natural antioxidant, emerged as a potential candidate for preventing oxidative degradation in different polymeric materials [34]. This [2-(3,4-dihydroxyphenyl)-5,7-dihydroxy-4*H*-chromen-4one)] is a flavanol type flavonoid found in fruits, vegetables, leaves and seeds and can be easily extracted through suitable solid phase extraction [35]. Till now, studies related to thermal kinetics have not been conducted by considering Quercetin as an antioxidant in UHMWPE.

In the present work, the thermal stability of UHMWPE samples blended with different concentrations (0.1–1.0 wt%) of Quercetin have been investigated (heating rate: 5 °C/min.) through the thermogravimetric (TGA/DTA) technique. The activation energies of these samples are also determined for different reaction mechanisms by adopting model fitting Coats and Redfern kinetic method. Further, thermograms of a maximum thermally stable sample are obtained at four different heating rates (5, 10, 15, 20 °C/min) and complexities involved during thermal degradation are resolved with deconvolution methods. Afterwards activation energies of deconvoluted peaks are determined by using both integral (Straink model) and differential (Friedman model) kinetic models. The reaction mechanism is identified using integral master plots and the pre-exponential factor is calculated with the help of activation energy and identified reaction mechanism. Finally, thermodynamic parameters, i.e., change in entropy (ΔS), change in enthalpy (ΔH) and change in Gibbs free energy (ΔG) are determined.

Materials and methodology

Material

UHMWPE (Ultra high molecular weight polyethylene) and Quercetin, in powder form, are procured from Sigma Aldrich, USA. The quoted molecular weight of UHMWPE is 3×10^6–6×10^6 g/mol and density is 0.94 g/ml. The purity of Quercetin powder is $\geq 95\%$ analyzed through High Performance Liquid Chromatography (HPLC).

Sample preparation

Quercetin (Q) with ten different weights ranging from 0.05 to 0.5 g, with interval of 0.05 g, is added in ethanol to prepare 1 wt% solution [36]. The solution (pale yellow

colour) is poured into UHMWPE powder to prepare ten different samples (UHMWPE-Q) with different concentrations (0.1–1.0 wt%). For proper homogenization of ethanolic-quercetin solution in UHMWPE matrix, stirring was done with the help of magnetic stirrer for 30 min. Then, mixture was dried in an oven at 50 °C to evaporate ethanol. Afterwards, dried UHMWPE-Q powder was kept in a desiccator loaded with anhydrous blue silica gel to further dry ethanol and moisture content, if any [37].

Moulding of sample

The dried UHMWPE-Q powder is compacted, in a cylindrical designed mould, at room temperature (25 °C) and 5 MPa pressure. Then, these samples are melted at an elevated temperature (140 °C) and compressed at 15 MPa pressure. Finally, UHMWPE-Q samples are gradually cooled with a dwelling time of 10 min and cylindrical shaped (diameter: 12 mm; height 40 mm) samples are prepared.

These UHMWPE-Q samples, with different quercetin concentrations, are cut into small pieces (~0.5 mm thickness; ~5 mg weight) for thermogravimetric analysis.

Thermogravimetric analysis (TGA) techniques

These samples are placed one by one in an alumina crucible and subjected to thermogravimetric analysis (Hitachi STA 7200 TGA analyzer). Thermograms (mass loss as a function of temperature) are recorded at 5 °C/min heating rate in temperature range 50–600 °C, in nitrogen environment at 100 ml/min gas flow rate. These thermograms are analyzed, through ORIGIN software, to identify the maximum thermally stable sample. This identified sample is further subjected to the thermogravimetric analysis at four different heating rates (5, 10, 15 and 20 °C/min) and mass loss as a function of temperature is recorded.

Theoretical kinetic approach

Kinetic models

Thermograms obtained through TGA/DTA technique are analyzed for kinetic studies [38]. For thermal degradation, the rate of reaction is described as:

$$\frac{d\alpha}{dt} = k(T)f(\alpha) \tag{1}$$

where $k(T)$ is the reaction rate constant, $f(\alpha)$ is the differential form of an ideal reaction model, T is the absolute temperature in Kelvin, t is the time duration of the reaction (in min) and α is the degree of conversion, which can be written as:

$$\alpha = \frac{m_o - m_t}{m_o - m_\infty} \tag{2}$$

where m_0 is the initial mass, m_t is the mass at time t, m_∞ is the final mass of the sample.

The rate constant $k(T)$ can be expressed by Arrhenius equation:

$$k(T) = Ae^{-E_a/RT} \tag{3}$$

$A\left(min^{-1}\right)$, $E_a(kJ/mol)$ and $R(8.314J/Kmol)$ are the pre-exponential factor, activation energy and gas constant, respectively.

By substituting the value of $k(T)$ in Eq. (1), one can write:

$$\frac{d\alpha}{dt} = Ae^{-E_a/RT}f(\alpha) \tag{4}$$

For non-isothermal TGA experiment, at linear heating rate $\beta = dT/dt$, the final equation for the rate of reaction can be obtained by modifying Eq. (4) as:

$$\frac{d\alpha}{dT} = \frac{A}{\beta}e^{-E_a/RT}f(\alpha) \tag{5}$$

By considering the above expression (5) as a base, different kinetic models are formulated [39–45]. These models follow different temperature integral approximations for the evaluation of kinetic parameters.

In the present study, Coats and Redfern (CR) [39] kinetic model is adopted to determine the activation energy of the considered samples. They utilized asymptotic series expansion [46, 47] and developed the following relation:

$$ln\left(\frac{g(\alpha)}{T^2}\right) = ln\left(\frac{AR}{\beta E_a}\right) + ln\left(1 - \frac{2RT}{E_a}\right) - \frac{E_a}{RT} \tag{6}$$

where $g(\alpha)$ is the integral form of an ideal reaction model. With the help of this model, the reaction mechanism is identified by plotting the different values of $g(\alpha)$ at different degree of conversion (α)(Table 1).

Deconvolution kinetic method

The second stage of thermal decomposition of UHMWPE (Figs. 2 and 3), with different quercetin concentrations, is very complex. To resolve this complexity, deconvolution kinetic method is adopted. In the present study, the deconvolution is performed by using the Bi-Gaussian asymmetric function:

$$y = \begin{pmatrix} y_0 + He^{-0.5\left(\frac{x-x_c}{w_1}\right)^2} for\, x < x_c \\ y_0 + He^{-0.5\left(\frac{x-x_c}{w_2}\right)^2} for\, x \geq x_c \end{pmatrix} \tag{7}$$

where y_0 is baseline, H is maximum height, x is the independent variable, x_c is the central value; w_1 and w_2 are the width of left and right side of the Gaussian peak.

The activation energy corresponding to each deconvoluted peak is determined for the second stage using ICTAC recommended iso-conversional [48] kinetic models.

Table 1 Reaction mechanisms involved in thermal decomposition processes in solids

Reaction Mechanism	$g(\alpha)$
n^{th} order reactions	
First order (F1)	$-ln(1-\alpha)$
Second order (F2)	$-1+(1-\alpha)^{-1}$
Third order (F3)	$0.5\left[-1+(1-\alpha)^{-2}\right]$
Diffusion mechanisms	
1D diffusion (D1)	α^2
2D diffusion (D2)	$\alpha+(1-\alpha)ln(1-\alpha)$
3D diffusion (Jander equation) (D3)	$\left[1-(1-\alpha)^{1/3}\right]^2$
3D diffusion (Ginstling-Brounshtein equation) (D4)	$1-(2/3)\alpha-(1-\alpha)^{2/3}$
Phase boundary reactions	
Cylinder symmetry (R2)	$1-(1-\alpha)^{1/2}$
Spherical symmetry (R3)	$1-(1-\alpha)^{1/3}$
Nucleation mechanisms	
Power law (P2)	$\alpha^{1/2}$
Power law (P3)	$\alpha^{1/3}$
Power law (P4)	$\alpha^{1/4}$
Power law (P2/3)	$\alpha^{3/2}$
Avrami-Erofeev (A2)	$[-ln(1-\alpha)]^{1/2}$
Avrami-Erofeev (A3)	$[-ln(1-\alpha)]^{1/3}$
Avrami-Erofeev (A4)	$[-ln(1-\alpha)]^{1/4}$

These are Starink (SR) integral kinetic model [44] and Friedman (FR) differential kinetic model [45]. Starink model is written as:

$$ln\left(\frac{\beta}{T^{1.92}}\right)=\ln\left(\frac{AR}{E_a}\right)+\ln\left(\frac{df(\alpha)}{d\alpha}\right)-1.0008\frac{E_a}{RT} \tag{8}$$

and Friedman kinetic model is written as:

$$ln\left(\beta\frac{d\alpha}{dT}\right)=lnA+lnf(\alpha)-\frac{E_a}{RT} \tag{9}$$

By using these models, activation energies are determined from the slopes obtained through the plots $ln\left(\beta/T^{1.92}\right)$ *vs.* $1000/T$ (Eq. 8) and $ln(\beta d\alpha/dt)$ *vs.* $1000/T$ (Eq. 9), respectively.

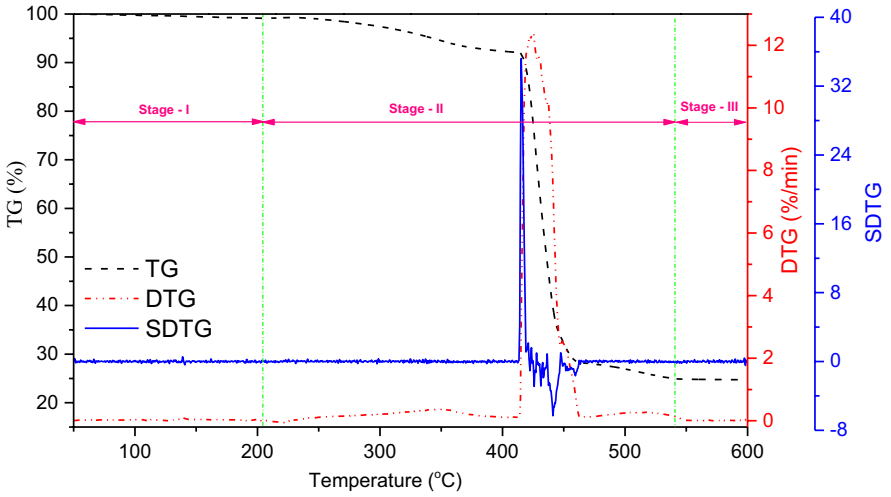

Fig. 1 Thermogravimetric (TG), its derivative (DTG) and Second Derivative (SDTG) curves of pure UHMWPE, at 5 °C/min heating rate

Result and discussion

Thermal decomposition behavior of UHMWPE

Fig. 1 presents the thermogravimetric (TG), its derivative (DTG) and second derivative (SDTG) curves of UHMWPE, which is compressed at optimized compression parameters (Temperature: 140 °C and Pressure: 15 MPa). Thermogram is recorded in temperature region 50–600 °C at 5 °C/min heating rate, in nitrogen environment. As per Fig. 1, UHMWPE shows three thermal decomposition stages. No noticeable mass loss is observed in Stage-I, which lies in the temperature region 50–208 °C. In the second stage (~ 208–539 °C), the mass gain is observed at ~ 233 °C temperature. Here, alkyl radicals ($R^{\bullet}$) combine with oxygen, present in the amorphous phase and form peroxy radicals ($ROO^{\bullet}$) [49–51].These peroxy radicals abstract hydrogen from adjacent hydrocarbon chains and convert into hydro-peroxide (ROOH) by forming alkyl radicals. These alkyl radicals further continue oxidative degradation. The O–O bond of peroxy-radical and hydroperoxide is relatively thermally unstable and breakdown into $RO^{\bullet}$ and OH, resulting in mass loss first slowly and then abruptly by forming low molecular weight carboxylic acid, alcohols, ketones, esters, water, olefins, paraffins etc. [52–54]. Around 468 °C, Diels–Alder Reaction favours the formation of cyclic products and as a result, unexpected mass gain is observed up to 539 °C. Second stage is highly active and variety of complex reactions are formed during thermal degradation, as clearly observed in SDTG curve (Fig. 1). In Stage-III, after 539 °C, sample is complete volatized and no loss in mass is observed.

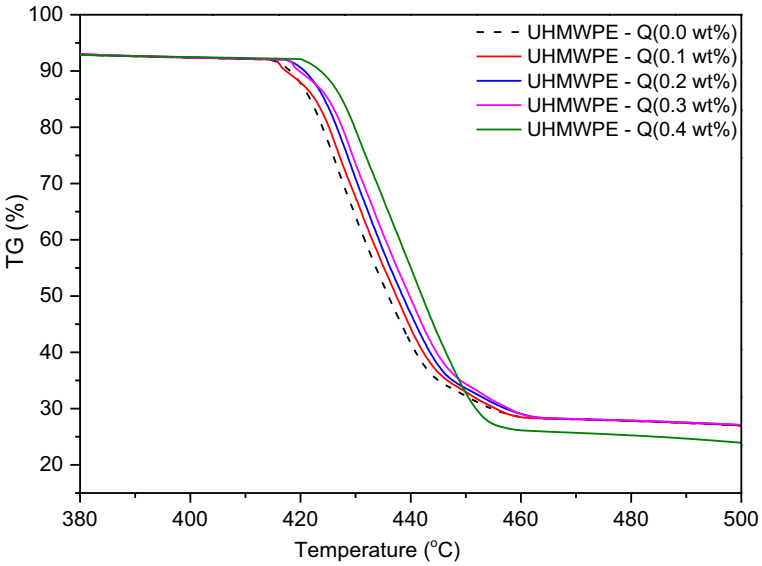

Fig. 2 TG/mass-loss curves of UHMWPE with different Quercetin (Q) concentration (0.0, 0.1, 0.2, 0.3, 0.4 wt%)

Table 2 Maximum decomposition temperature (T_{max}) of Stage-II at different Quercetin concentrations

Quercetin concentration (wt%)	T_{max} (°C)
0.0	431
0.1	432
0.2	433
0.3	435
0.4	438
0.5	436
0.6	435
0.7	434
0.8	430
0.9	428
1.0	427

Optimization of quercetin concentration in UHMWPE through thermal stability

To observe the impact of quercetin concentrations on thermal stability of UHMWPE, recorded thermograms (at 5 °C/min heating rate) are presented in Fig. 2 and Fig. S1a, b. These thermograms show similar thermal decompositions stages as observed in pure UHMWPE (Fig. 2). However, the maximum decomposition temperature (T_{max}) is different at different quercetin concentrations (Table 2). Firstly, thermal stability increases with an increase in quercetin concentration up

to 0.4 wt% (Fig. 2); then it decreases with an increase of concentration from 0.5 to 0.7 wt% (Fig. S1a) and finally, it decreases even below the pure UHMWPE (Fig. S1b). The enhancement in thermal stability up to 0.4 wt% may be due to scavenging of formed free radicals of UHMWPE by abstracting hydrogen from the hydroxyl group of quercetin, leave phenoxy radicals of quercetin that can be further stabilized by delocalization of their electrons and forms various stable aromatic compounds of low molecular weight. However, an increase in quercetin concentration (0.5–0.7 wt%) lowers its efficiency as radical scavenger. This might be due to the reaction of quercetin directly with the oxygen present in UHMWPE. Here, in concentration 0.1–0.7 wt%, quercetin acts as antioxidant in UHMWPE. At higher concentration (0.8–1.0 wt%), quercetin transformed into pro-oxidant by forming various oxidative products [55], resulting in even lower thermal stability of pure UHMWPE. The above discussion reveals that quercetin act as antioxidant at lower concentration only and observed maximum thermal stability of UHMWPE at 0.4 wt%.

To ascertain that maximum thermal stability of UHWMPE at 0.4 wt% quercetin only, activation energy at different quercetin concentration for different reaction mechanisms are obtained (Table 3) by utilizing Coats and Redfern Kinetic model. The table also revealed that values of activation energy are maximum at 0.4 wt% as compared to other concentrations.

Table 3 Activation energies (kJ/mol) at different quercetin concentrations, for different reaction mechanisms, obtained through Coats and Redfern model

Reaction mechanism	0.0	0.1	0.2	0.3	0.4	0.5	0.6	0.7	0.8	0.9	1.0
F1	462	507	514	519	652	516	515	511	456	446	440
F2	607	669	673	682	870	682	680	672	579	564	560
F3	789	863	866	872	1136	871	869	868	727	707	691
D1	721	788	793	799	989	796	790	769	667	650	644
D2	781	860	863	873	1085	872	888	834	722	683	672
D3	854	947	958	976	1202	972	965	945	788	747	742
D4	802	879	882	889	1125	890	881	865	745	713	704
R2	401	441	453	460	561	455	450	448	398	397	390
R3	413	462	472	479	591	473	471	467	405	402	392
P2	167	180	201	223	231	228	221	229	147	127	121
P3	102	111	142	159	165	155	147	163	95	93	93
P4	78	79	86	92	105	90	87	82	71	63	61
P2/3	538	586	589	594	736	598	592	578	514	493	489
A2	140	218	232	243	315	241	238	232	132	127	123
A3	101	153	157	158	201	152	147	149	95	89	83
A4	213	246	267	278	298	272	266	263	208	201	196

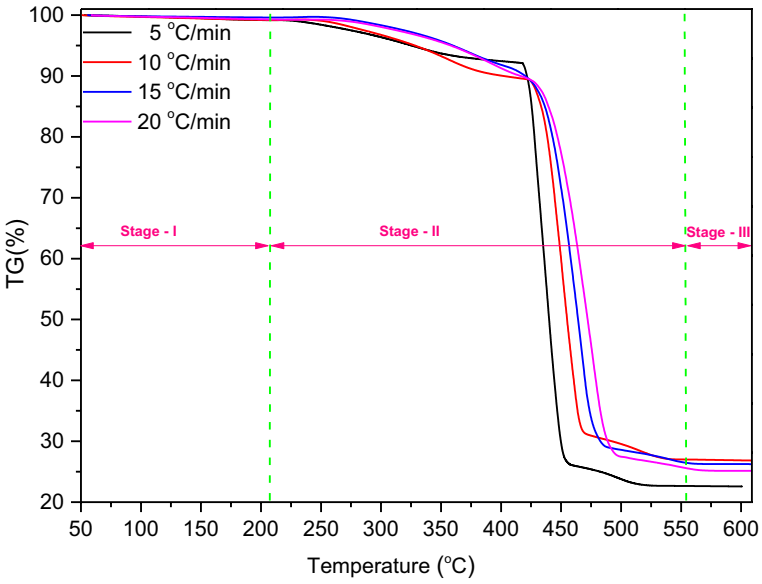

Fig. 3 TG/mass-loss curves of UHMWPE + Quercetin (0.4 wt%) at four different heating rates (5, 10, 15 and 20 °C/min)

Thermal kinetic parameters of UHMWPE at optimized quercetin concentration

In order to explore different thermal kinetic parameters, thermograms of UHMWPE with quercetin (0.4 wt% concentration) are obtained at four different heating rates (5, 10, 15, 20 °C/min.) and are presented in Fig. 3. It is observed that these TG curves are of similar trend and shows three decomposition stages in which Stage-II is highly active and complex. In addition, TG curves also shifted towards higher temperature side with an increase in heating rate. Similar trends are also observed in plots (Fig. S2a, b) of the degree of conversion (α) and change of degree of conversion ($d\alpha/dt$) as a function of temperature. This may be due to the delay participation of radicals, in thermal decomposition, resulting in thermal lag, which leads to a change in thermal kinetic parameters. Further, peaks (Fig. S2b) also reveal the complexities involved in thermal reactions in Stage-II.

Deconvolution kinetic method

The complexities involved in thermal reactions (Stage-II) are resolved through deconvolution method. Adopting this, peaks are deconvoluted by applying the Bi-Gaussian asymmetric function (Eq. 7). At 5 °C/min heating rate, two peaks at two different temperatures (432 and 444 °C) are obtained (Fig. 4). Similar trends are also observed (two peaks at two different temperatures) for other heating rates after deconvolution (Fig. S3a–c). These peaks are presented separately in Fig. 5a, b. Further, degree of conversion (α) values are generated and presented as a function of

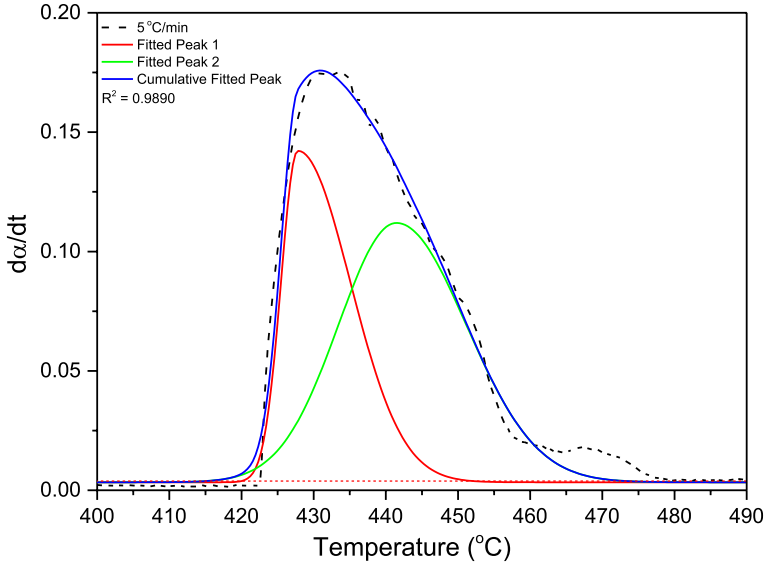

Fig. 4 Deconvoluted peaks in Stage-II of UHMWPE + Quercetin (0.4 wt%) at 5 °C/min heating rate

temperature at different heating rates (Fig. S4a, b). Figs. 5 and S4) reveals that peaks are shifted towards higher temperatures, which substantiates the thermal lagging.

Estimation of activation energy

To estimate activation energies for Peak 1 and Peak 2, linear fitted plots are generated at different conversion values (Fig. S4a, b) by adopting Starink (Fig. 6a, b) and Friedman (Fig. S5a, b) models. The obtained linear fitted parameters (slope, standard error (S.E.), R^2 value) and activation energy are given in Tables 4 and 5. It is observed that the values of activation energies based on Starink model are less as compared to Friedman model. Further, the activation energy value of Peak 1 decrease with increase in degree of conversion (α) value while for Peak 2 it increases for both integral and differential models.

Determination of specific reaction mechanism

The reaction mechanism involved in thermal decomposition of the considered sample (UHMWPE + quercetin (0.4 wt%)) is determined through integral master plots method. As per this method, thermal decomposition reaction can be expressed [56] as:

$$g(\alpha) = \frac{AE_a}{\beta R} P(u) \tag{10}$$

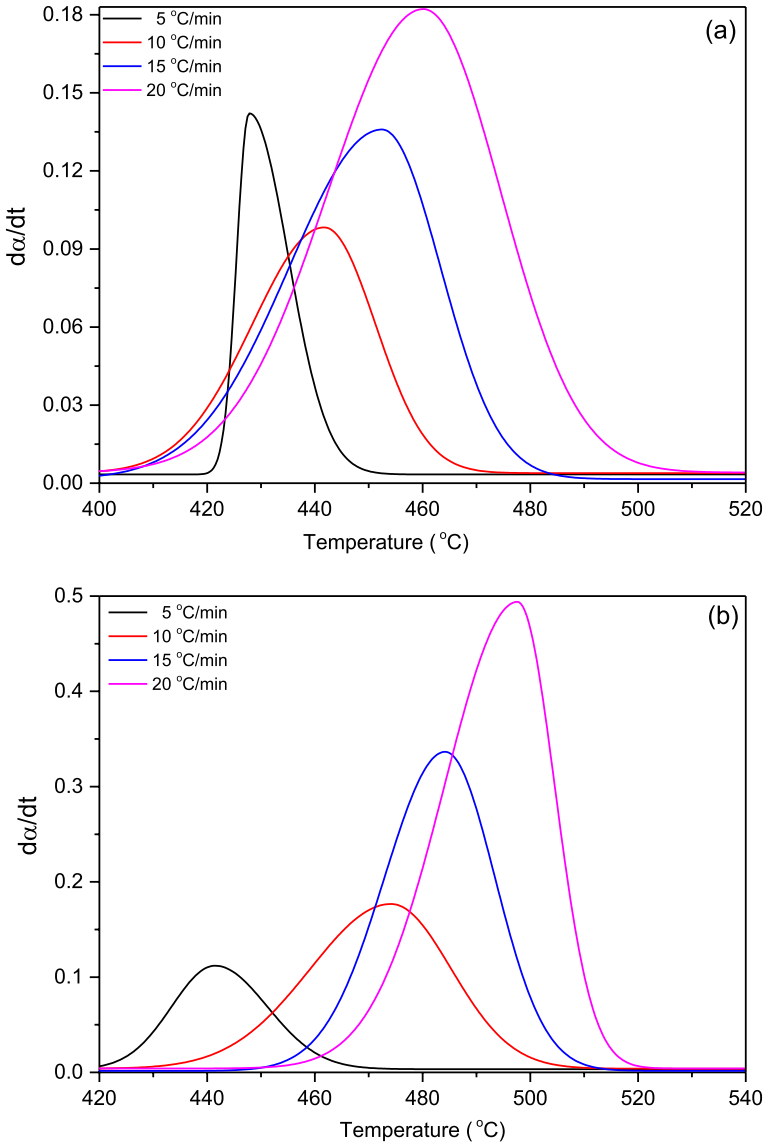

Fig. 5 $d\alpha/dt$ as a function of Temperature in Stage-II of UHMWPE + Quercetin (0.4 wt%) for **a** Peak 1 and **b** Peak 2, at different heating rates

where $g(\alpha)$ is the integral function at different degree of conversion (α),$u = E_a/RT$ and $P(u)$ is the temperate integral that can be expressed as:

$$P(u) \approx \frac{e^{(-1.0008u-0.312)}}{u^{0.92}} \tag{11}$$

To determine reaction mechanism, the above expression can be expressed as

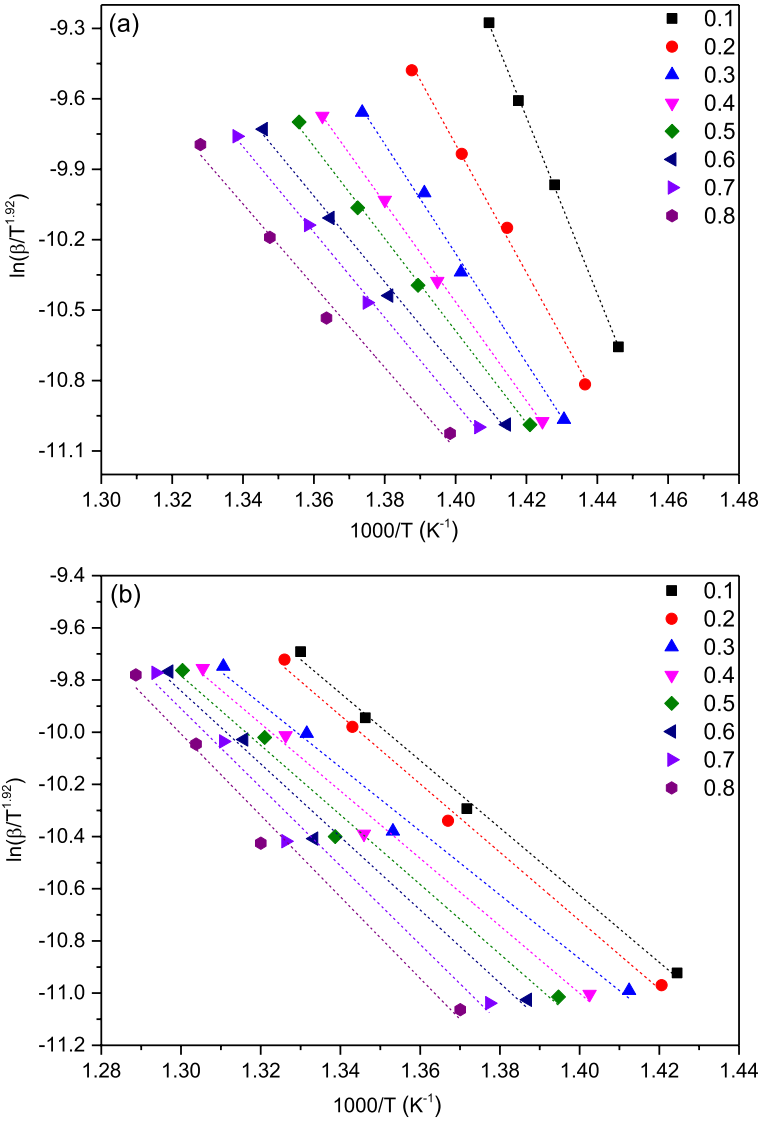

Fig. 6 Linear fitted curves at different conversion values obtained through Starink model for **a** Peak 1 and **b** Peak 2

$$\frac{g(\alpha)}{g(0.5)} = \frac{P(u)}{P(0.5)} \tag{12}$$

By utilizing Starink model-based activation energy, experimental values are generated and presented as a function of the degree of conversion (α) at different heating rates (Figs. 7, 8, S6 and S7). Further, master plots are generated for different reaction mechanisms (Table 1) and introduced in these figures. The

Table 4 Linear fitting parameters obtained through Starink model for Peak 1 and Peak 2

Peak 1					Peak 2			
α	Slope	S.E	R^2	E_a(kJ/mol)	Slope	S.E	R^2	E_a(kJ/mol)
0.1	– 37.574	0.484	0.999	312	– 12.896	0.494	0.995	107
0.2	– 27.326	1.058	0.995	227	– 13.098	0.617	0.993	109
0.3	– 23.289	1.191	0.992	193	– 12.223	0.899	0.983	102
0.4	– 21.052	0.389	0.999	175	– 12.921	1.002	0.982	107
0.5	– 19.643	0.497	0.998	163	– 13.331	1.180	0.976	111
0.6	– 18.283	0.695	0.995	152	– 13.992	1.215	0.977	116
0.7	– 18.196	0.480	0.997	151	– 15.059	1.472	0.971	125
0.8	– 17.404	1.331	0.982	145	– 15.623	1.432	0.975	130

Table 5 Linear fitting parameters obtained from Friedman model for Peak 1 and Peak 2

Peak 1					Peak 2			
α	Slope	S.E	R^2	E_a(kJ/mol)	Slope	S.E	R^2	E_a(kJ/mol)
0.1	– 52.093	0.822	0.999	433	– 13.944	0.289	0.998	116
0.2	– 36.978	3.719	0.952	307	– 10.795	1.918	0.910	90
0.3	– 24.034	1.197	0.992	200	– 12.666	1.322	0.967	105
0.4	– 20.120	0.296	0.999	167	– 14.783	1.171	0.981	123
0.5	– 17.776	0.357	0.999	148	– 14.886	1.098	0.983	124
0.6	– 17.190	0.872	0.992	143	– 15.251	2.366	0.931	127
0.7	– 17.504	1.421	0.980	146	– 17.316	3.230	0.902	144
0.8	– 17.084	1.035	0.989	142	– 18.903	1.246	0.987	157

comparison between experimental values and master plots reveals that Peak 1 and Peak 2 favours A2 and A3 (random nucleation) reaction mechanisms, respectively. These reaction mechanisms may be due to semi-crystalline nature of UHMWPE, which restricts the mobility of free radicals in amorphous phases and facilitate random nucleation [57].

Estimation of pre-exponential factor and thermodynamic parameters

For determination of pre-exponential factors (A), Eq. (10) is rewritten by replacing $g(\alpha)$ with A2 reaction mechanism for Peak 1 (Eq. 13) and A3 reaction mechanism for Peak 2 (Eq. 14) as

$$[-ln(1-\alpha)]^{1/2} = \frac{AE_a}{\beta R}P(u) \tag{13}$$

and

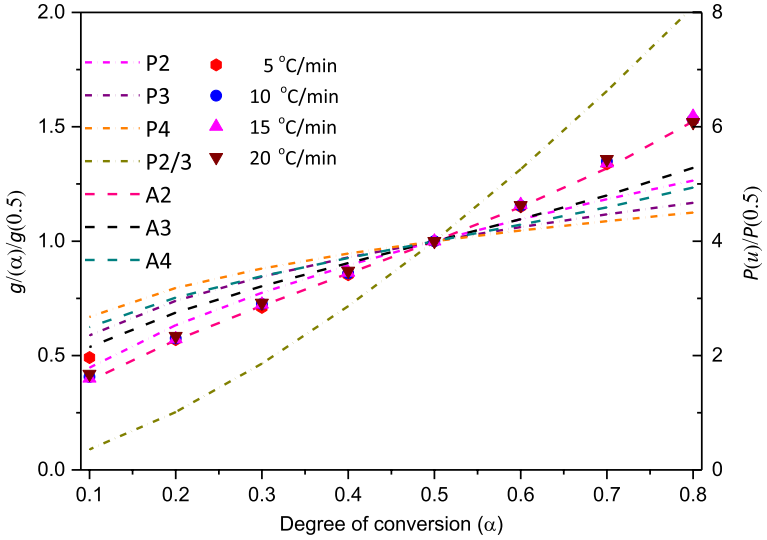

Fig. 7 Comparison between experimental values (represented with symbols) and theoretical master curves obtained for different nucleation mechanisms, for Peak 1

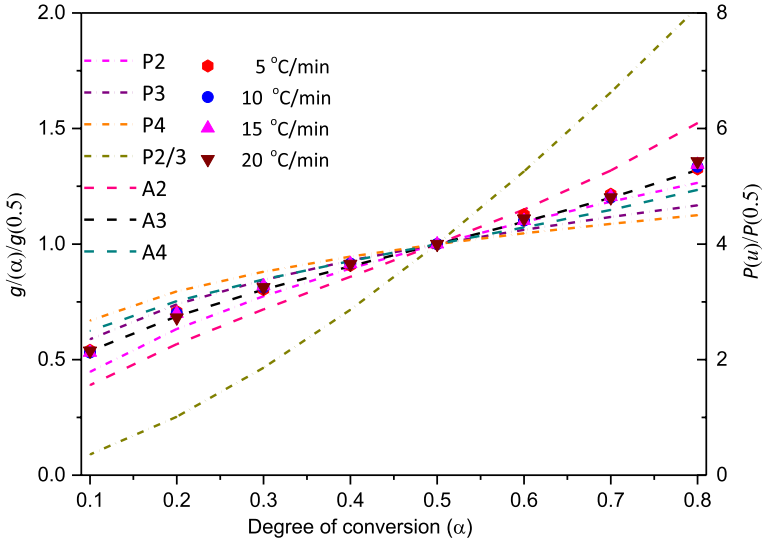

Fig. 8 Comparison between experimental values (represented with symbols) and theoretical master curves obtained for different nucleation mechanisms, for Peak 2

Table 6 Pre-exponential factor and thermodynamic parameters of Peak 1 at different heating rates

Heating rate (°C/min)	T_{max} (°C)	A (1/min)	ΔS (J/mol/K)	ΔH (kJ/mol)	ΔG (kJ/mol)
5	428	2.90×10^{8}	− 98.33	131.47	200.40
10	442	3.15×10^{8}	− 97.80	130.30	200.23
15	452	3.33×10^{8}	− 97.46	129.47	200.13
20	460	3.47×10^{8}	− 97.21	128.81	200.06

Table 7 Pre− exponential factor and thermodynamic parameters of Peak 2 at different heating rates

Heating rate (°C/min)	T_{max} (°C)	A (1/min)	ΔS (J/mol/K)	ΔH (kJ/mol)	ΔG (kJ/mol)
5	442	1.69×10^{7}	− 122.12	53.93	141.25
10	475	1.79×10^{7}	− 122.02	51.19	142.46
15	485	2.25×10^{7}	− 120.23	50.35	141.49
20	498	2.34×10^{7}	− 120.05	49.27	141.83

$$[-ln(1-\alpha)]^{1/3} = \frac{AE_a}{\beta R}P(u) \tag{14}$$

By plotting linear fitted curves between $[-ln(1-\alpha)]^{1/2}$ and $\left(E_a/\beta R\right)P(u)$ for Peak 1 and $[-ln(1-\alpha)]^{1/3}$ and $\left(E_a/\beta R\right)P(u)$ for Peak 2, pre-exponential factors at different heating rate are determined and given in Tables 6 and 7.

For thermodynamic parameters [58, 59] viz. entropy change (ΔS), enthalpy change (ΔH), and Gibbs free energy change (ΔG), the following equations are utilized:

$$\Delta \mathrm{S} = Rln\left(\frac{Ah}{e\varkappa k_b T_{max}}\right) \tag{15}$$

$$\Delta \mathrm{H} = E_a - RT_{max} \tag{16}$$

and

$$\Delta \mathrm{G} = \Delta \mathrm{H} - T_{max}\Delta \mathrm{S} \tag{17}$$

where e, $\varkappa$, k_b and h are Neper number (2.7183), transition number (Equal to unity for monomolecular reaction), Boltzmann's constant (1.38×10^{-23} Js^{-1}) and Planck's constant (6.626×10^{-34} Js^{-1}), respectively. By utilizing maximum decomposition temperature $\left(T_{max}\right)$ in these equations, values of considered thermodynamic parameters are determined (Tables 6 and 7). It is observed from these tables that ΔS values are negative and values of ΔG and ΔH are positive for both the peaks. This reveals that the thermal decomposition of UHMWPE + Quercetin (0.4 wt%) is endergonic, non-spontaneous and unfavourable.

Conclusions

The thermal decomposition of UHMWPE shows three decomposition stages and Stage-II (~208–539 °C) is highly complex and active. Mixing of quercetin in UHMWPE matrix doesn't alter the decomposition stages. However, the temperature regions of decomposition stages are varied. At low (up to 0.7 wt%) concentration, quercetin acts as an antioxidant in UHMWPE matrix whereas it behaves as a pro-oxidant at higher concentration (0.8–1.0 wt%). Further, at 0.4 wt% quercetin concentration thermal stability of UHMWPE is maximum. Complexities involved in Stage-II are resolved through deconvolution by splitting into two peaks. Obtained activation energies, through integral (Starink) and differential (Friedman) kinetic models, at different heating rates are higher for Peak 1 than Peak 2. Here, random nucleation reaction mechanism favours the thermal decomposition. Additionally, negative value of change in entropy (ΔS) and positive value of change in enthalpy (ΔH) and change in Gibbs free (ΔG) energy indicates that thermal decomposition of UHMWPE is non-spontaneous and endergonic. The study brings new prospects for optimizing minimal quercetin concentration to provide maximum thermal stability to UHMWPE for higher temperature applications.

Supplementary Information The online version contains supplementary material available at https://doi.org/10.1007/s11144-023-02472-2.

Data availability Data will be made available on request.

Declarations

Conflict of interest The authors declare that they have no known competing financial interests or personal relationships that could have appeared to influence the work reported in this paper.

References

1. Gonchikzhapov MB, Paletsky AA, Kuibida LV, Shundrina IK, Korobeinichev OP (2012) Reducing the flammability of ultra-high-molecular-weight polyethylene by triphenyl phosphate additives. Combust Explos Shock Waves 48(5):579–589
2. Laska A (2017) Comparison of conventional and crosslinked ultra high molecular weight polyethylene (UHMWPE) used in hip implant. World Sci News 73(1):51–60
3. Azam AM, Mehmood MS (2017) Thermal stability of ultra high molecular weight polyethylene nano composites with $Mg_{0.15}Ni_{0.15}$ $Zn_{0.70}Fe_2O_3$. J Mater Phys Chem 5(1):39–42
4. Bracco P, Bellare A, Bistolfi A, Affatato S (2017) Ultra-high molecular weight polyethylene: influence of the chemical, physical and mechanical properties on the wear behavior—a review. Materials 10(7):791
5. Mukhtar SS, Mehmood MS, Maqbool SA, Ghafoor B, Baluch MA, Siddiqui N, Yasin T (2018) Effect of γ-irradiation on the thermal properties of UHMWPE/MWCNTs nanocomposites: a comparative study of incorporating unmodified and γ-ray-modified MWCNTs. Bull Mater Sci 41:10
6. Dayyoub T, Maksimkin AV, Kaloshkin S, Kolesnikov E, Chukov D, Dyachkova TY, Gutnik I (2019) The structure and mechanical properties of the UHMWPE films modified by the mixture of graphene nanoplates with polyaniline. Polymers 11:23
7. Sobieraj MC, Rimnac CM (2009) Ultra high molecular weight polyethylene: mechanics, morphology, and clinical behavior. J Mech Behav Biomed Mater 2:433–443

8. Hofste JM, Van Voorn B, Pennings AJ (1997) Mechanical and tribological properties of short discontinuous UHMWPE fiber reinforced UHMWPE. Polym Bull 38:485–492
9. Xue Y, Wu W, Jacobs O, Schädel B (2006) Tribological behaviour of UHMWPE/HDPE blends reinforced with multi-wall carbon nanotubes. Polym Test 25:221–229
10. Plumlee K, Schwartz CJ (2009) Improved wear resistance of orthopaedic UHMWPE by reinforcement with zirconium particles. Wear 267:710–717
11. Guofang G, Huayong Y, Xin F (2004) Tribological properties of kaolin filled UHMWPE composites in unlubricated sliding. Wear 256:88–94
12. Kurtz S (2004) The UHMWPE Handbook: Ultra-High Molecular Weight Polyethylene Total Joint Replacement. Elsevier
13. Yun DW, Jang J (2014) Wear minimization of ultra high molecular weight polyethylene by benzophenone-assisted photo crosslinking Fibers. Polym 15(3):480–486
14. Wen X, Li Z, Yang C, Yan K, Wu G, Wang D (2022) Electron beam irradiation assisted preparation of UHMWPE fibre with 3D cross-linked structure and outstanding creep resistance. Radiat Phys Chem 199:110370
15. Wang H, Xu L, Hu J, Wang M, Wu G (2015) Radiation-induced oxidation of ultra-high molecular weight polyethylene (UHMWPE) powder by gamma rays and electron beams: a clear dependence of dose rate. Radiat Phys Chem 115:88–96
16. Wu X, Wu C, Wang G, Jiang P, Zhang J (2013) A crosslinking method of UHMWPE irradiated by electron beam using TMPTMA as radio sensitizer. J Appl Polym Sci 127:111–119
17. Ikada Y, Nakamura K, Ogata S, Makino K, Tajima K, Endoh N, Hayashi T, Fujita S, Fujisawa A, Masuda S, Oonishi H (1999) Characterization of ultrahigh molecular weight polyethylene irradiated with γ-rays and electron beams to high doses. J Polym Sci Part A: Polym Chem 37:159–168
18. Bracco P, Brunella V, Luda MP, Zanetti M, Costa L (2005) Radiation-induced crosslinking of UHMWPE in the presence of co-agents: chemical and mechanical characterisation. Polymer 46:10648–10657
19. Oral E, Ghali BW, Muratoglu OK (2011) The elimination of free radicals in irradiated UHMWPEs with and without vitamin E stabilization by annealing under pressure. J Biomed Mater Res Part B Appl Biomater 97:167–174
20. Ferroni D, Quaglini V (2010) Thermal stabilization of highly crosslinked UHMWPE: a comparative study between annealed and remelted resins. J Appl Biomater Biomech 8:82–88
21. Visco AM, Campo N, Brancato V, Trimarchi M (2013) Influence of α-tocopherol load and annealing treatment on the wear resistance of biomedical UHMWPE irradiated with electron beam. Int J Polym Anal Charact 18:545–556
22. Ors-Unsal A, Archodoulaki VM (2020) Comparison of in-vivo performance characteristics of first and second-generation cross-linked and conventional explants. J Arthroplasty 35:3330–3337
23. Helberg J, Pratt DA (2021) Autoxidation vs. antioxidants–the fight for forever. Chem Soc Rev 50:7343–7358
24. Hope N, Bellare A (2015) A comparison of the efficacy of various antioxidants on the oxidative stability of irradiated polyethylene. Clin Orthop Relat Res 473:936–941
25. Allam SS, Mohamed HM (2002) Thermal stability of some commercial natural and synthetic antioxidants and their mixtures. J Food Lipid 9:277–293
26. Narayan VS (2015) Spectroscopic and chromatographic quantification of an antioxidant-stabilized ultrahigh-molecular-weight polyethylene. Clin Orthop Relat Res 473:952–959
27. Xiao C, Zhang Y, An S, Jia G (2000) Effects of phenolic antioxidants on ultrahigh molecular weight polyethylene/decalin solution. J Appl Polym Sci 77:2877–2881
28. Bolbukh Y, Kuzema P, Tertykh V, Laguta I (2008) Thermal degradation of polyethylene containing antioxidant and hydrophilic/hydrophobic silica. J Therm Anal Calorim 94:727–736
29. Wolf C, Krivec T, Blassnig J, Lederer K, Schneider W (2002) Examination of the suitability of α-tocopherol as a stabilizer for ultra-high molecular weight polyethylene used for articulating surfaces in joint endoprostheses. J Mater Sci Mater Med 13:185–189
30. Bracco P, Brunella V, Zanetti M, Luda MP, Costa L (2007) Stabilisation of ultra-high molecular weight polyethylene with vitamin E. Polym Degrad Stab 92:2155–2162
31. Souza VC, Santos EB, Mendonça AV, Silva LB (2018) Thermal behaviour and decomposition kinetic studies of biomedical UHMWPE/vitamin C compounds. J Therm Anal Calorim 134:2097–2105

32. Fu J, Shen J, Gao G, Xu Y, Hou R, Cong Y, Cheng Y (2013) Natural polyphenol-stabilised highly crosslinked UHMWPE with high mechanical properties and low wear for joint implants. J Mater Chem B 1:4727–4735
33. Costa L, Carpentieri I, Bracco P (2009) Post electron-beam irradiation oxidation of orthopaedic Ultra-High Molecular Weight Polyethylene (UHMWPE) stabilized with vitamin E. Polym Degrad Stab 94:1542–1547
34. Tátraaljai D, Földes E, Pukánszky B (2014) Efficient melt stabilization of polyethylene with quercetin, a flavonoid type natural antioxidant. Polym Degrad Stab 102:41–48
35. Molinelli A, Weiss R, Mizaikoff B (2002) Advanced solid phase extraction using molecularly imprinted polymers for the determination of quercetin in red wine. J Agric Food Chem 50:1804–1808
36. Kang X, Zong X, Zhang P, Zeng X, Liu Y, Yao C, Wang T, Feng P, Yang C (2021) Effects of epigallocatechin gallate incorporation in UHMWPE on biological behavior, oxidative degradation, mechanical and tribological performance for biomedical applications. Tribol Int 158:106887
37. Van Mourik JH (1965) Experiences with silica gel as adsorbent. Am Ind Hyg Assoc J 26:498–509
38. Haines PJ (1995) Thermal Methods of Analysis: Principles, Applications and Problems. Blackie Academic & Professional, Dordrecht
39. Coats AW, Redfern JP (1964) Kinetic parameters from thermogravimetric data. Nature 201:68–69
40. Flynn JH, Wall LA (1966) A quick, direct method for the determination of activation energy from thermogravimetric data. J Polym Sci B: Polym Lett 4(1966):323–328
41. Ozawa T (1965) A new method of analyzing thermogravimetric data. Bull Chem Soc Jpn 38:1881–1886
42. Kissinger HE (1957) Reaction kinetics in differential thermal analysis. Anal Chem 29(11):1702–1706
43. Akahira TJ, Sunose T (1971) Method of determining activation deterioration constant of electrical insulating materials. Res Rep Chiba Inst Technol 16:22–31
44. Starink MJ (2003) The determination of activation energy from linear heating rate experiments: a comparison of the accuracy of isoconversion methods. Thermochim Acta 404:163–176
45. Friedman HL (1964) Kinetics of thermal degradation of char-forming plastics from thermogravimetry: application to a phenolic plastic. J Polym Sci Part C, Polym Symp 6:183–195
46. Norwisz J, Hajduk N (1978) The accuracy of equations approximating the temperature integral part I. J Therm Anal 13:223–230
47. Hajduk N, Norwisz J (1979) The accuracy of equations approximating the temperature integral. Part II J Therm Anal 16:193–195
48. Vyazovkin S, Burnham AK, Criado JM, Pérez-Maqueda LA, Popescu C, Sbirrazzuoli N (2011) ICTAC kinetics committee recommendations for performing kinetic computations on thermal analysis data. Thermochim Acta 520:1–19
49. Martínez-Morlanes MJ, Medel FJ, Mariscal MD, Puértolas PJA (2010) On the assessment of oxidative stability of post-irradiation stabilized highly crosslinked UHMWPEs by thermogravimetry. Polym Test 29:425–432
50. Bracco P, Del Prever EB, Cannas M, Luda MP, Costa L (2006) Oxidation behaviour in prosthetic UHMWPE components sterilised with high energy radiation in a low-oxygen environment. Polym Degrad Stab 91:2030–2038
51. Shafiq M, Mehmood MS, Yasin T (2013) On the structural and physicochemical properties of gamma irradiated UHMWPE/silane hybrid. Mater Chem Phys 143:425–433
52. Costa L, Bracco P (2016) Mechanisms of cross-linking, oxidative degradation, and stabilization of UHMWPE. In: UHMWPE Biomaterials Handbook. William Andrew Publishing, Philadelphia
53. Singh RK, Ruj B, Sadhukhan AK, Gupta P (2017) Impact of fast and slow pyrolysis on the degradation of mixed plastic waste: product yield analysis and their characterization. J Energy Inst 92:1647–1657
54. Kumar S, Panda AK, Singh RK (2011) A review on tertiary recycling of high-density polyethylene to fuel. Resour Conserv Recycl 55:893–910
55. Padrón AJ, Colmenares MA, Rubinztain Z, Albornoz LA (1987) Influence of additives on some physical properties of high density polyethylene-I. Commercial antioxidants Eur Polym J 23:723–727
56. Sharma P, Kaur T, Pandey OP (2019) In situ single-step reduction and silicidation of MoO_3 to form $MoSi_2$. J Am Ceram 102:1522–1534

57. Xu J, Reiter G, Alamo RG (2021) Concepts of nucleation in polymer crystallization. Crystals 11:304
58. Georgieva V, Zvezdova D, Vlaev L (2013) Non-isothermal kinetics of thermal degradation of chitin. J Therm Anal Calorim 111:763–771
59. Sharma P, Pandey OP, Diwan PK (2019) Non-isothermal kinetics of pseudo-components of waste biomass. Fuel 253:1149–1161